

# Deep Learning Technology-Based Exoskeleton Robot Controller Development

SK Hasan

Department of Mechanical and Manufacturing Engineering

Miami University

Oxford, OH 45056

**Word count:** 5,123

**Corresponding Author:**

**SK Hasan**

[hasansk@miamioh.edu](mailto:hasansk@miamioh.edu)

Department of Mechanical and Manufacturing Engineering

Miami University

Oxford, OH

OH 45056

# Deep Learning Technology-Based Exoskeleton Robot Controller Development

## Abstract:

Model-based control is common for robotics applications. The fundamental challenge in implementing a model-based controller for higher degrees of freedom robot is it requires higher computational power to compute mass, gravity, and Coriolis-centrifugal force in real-time. For higher degrees of freedom robot, mass matrix, Coriolis and centrifugal force and gravity matrix are computationally heavy and require a long time to execute. Due to the sequential structure of the programs, multicore processors cannot boost performance. High processing power is required to maintain a higher sampling rate. Neural network-based control is a great approach for developing a parallel equivalent model of a sequential model. In this paper, Deep learning algorithm-based controller is designed for 7 degrees of freedom exoskeleton robot. A total of 49 densely connected neurons are arranged in four layers to estimate joint torque requirements for tracking trajectories. For training, the deep neural network analytical model-based data generation technique is presented. A PD controller is added to handle prediction errors. Since a deep learning network has a parallel structure, using a multicore CPU/GPU can significantly improve the controller performance. Simulation results show very high trajectory tracking accuracies. The developed controller's stability analysis is presented. The robustness of the controller to the parameters variation is analyzed with the help of the analysis of variance (ANOVA). A comparative study between the developed controller and the Sliding Mode Controller, Computed Torque Controller, Adaptive controller, Linear Quadratic Regulator, and Model Reference Computed Torque Controller are discussed while keeping the same robot dynamics.

**Keywords:** Deep learning robot control, Exoskeleton robot control, AI in dynamic control

# Exoskeleton Robot Controller Development Based on Deep Learning Technology

## 1. Introduction

Our daily lives are being overtaken by robots. Robotic applications are not limited to a specific field. Currently, robots are widely used in industrial automation [1], healthcare system [2], space exploration [3], agriculture [4], underwater exploration [5], food pre-post-processing applications [6], manufacturing technology [7, 8], military application [9], human power assistance and rehabilitation applications [10-12]. Industry 4 Smart factory technology heavily relies on robots [13]. Improving robot control technology has a great impact on society.

Robotics is an interdisciplinary branch of engineering, which combines electrical, mechanical, computer and control system technology. The accuracy, precision, and usability of a robot highly depend on the motion control system. Figure 1 presents the Mechatronics architecture of a robot.

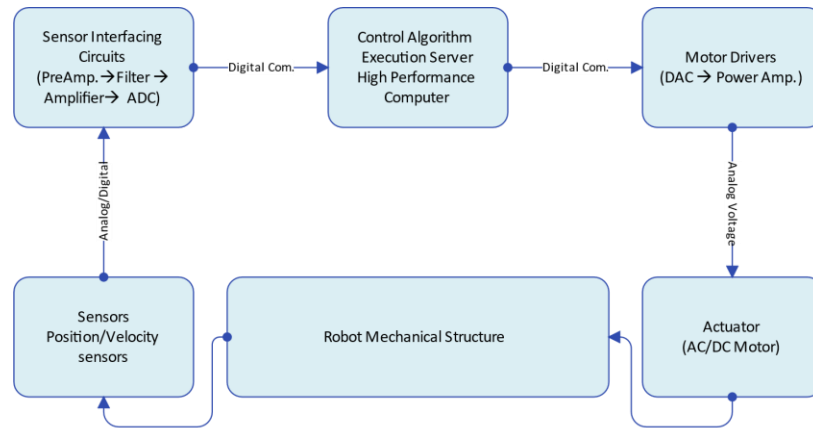


Figure 1 Mechatronics architecture of a robot

Model-based control is very common in robotics applications [14]. Both kinematic and dynamic model is widely used for controlling the robot. There are two common techniques used for developing the robot dynamic equation of motion are Newton-Euler's method and the Lagrange energy method [15]. The final dynamic equation of motion is independent of the method used for developing the dynamics. Robot dynamics is nonlinear. The major sources of nonlinearities are gravity, Coriolis and centrifugal forces, and the joint friction forces. The dynamic model allows to separate the sources of nonlinearities from the dynamic system.

The robot dynamic model is composed of the mass, gravity, Coriolis-centrifugal force matrices, and friction model. During the linearization process, the gravity, Coriolis and centrifugal forces, and joint friction forces are computed separately and feedback to the robot dynamic model. After linearization, the

linear/angular acceleration of a joint becomes proportional to the applied force or torques, and the mass matrix acts as the proportional constant. Any linear control scheme can be employed to control the robot dynamics. The whole process is called model-based control. Some widely used model-based robot control schemes are Computer torque control [16], Adaptive control [17], Model reference computed torque control [18], etc. It is challenging to determine the robot parameters accurately, so the robot controller needs to be robust enough to handle the parametric uncertainties.

For a higher degree of freedom robot, the dynamics are complicated. The mass, gravity, and Coriolis-centrifugal matrices become computationally heavy. Most of the robot control algorithms are based on torque control techniques which require a higher sampling rate than the position or velocity control scheme. High computational power is required to complete the execution within the sampling period. The mass, gravity, and Coriolis-centrifugal matrices are sequentially structured. Multicore CPU or GPU neither boost the performance nor reduce the execution time. There are different robot control techniques available. Linear [16, 19], nonlinear [18], robust [20], optimal [19], adaptive control [17] schemes can be used for controlling a robot. By analyzing the established control techniques [16-20] it has been noticed that most of them are based on model-based control techniques. Different parts of the robot's dynamic equation of motion are used for linearization and control. The internal architecture of robot dynamics is shown in Figure 4.

Deep learning is a well-established technique for solving classification and prediction problems [21]. Deep learning technology is used widely for a variety of applications. Dragan et al. presented more details about different applications of the deep neural network [22]. The deep neural network is based on parallel architecture. Deep learning technology is the successor of shallow neural networks. A good number of research works have been conducted on using neural networks for robot dynamic modeling and control. Some prominent works that used neural networks for robot control applications are discussed below.

Chen et al. [23] combined the iterative learning control and neural network to improve the trajectory tracking accuracy of multi degrees of freedom industrial robots. They identified the robot's internal dynamics using physical stimulations and developed a neural network to model the robot internal dynamics. Finally, to compensate for the robot's internal dynamics and time delay of a robot, a neural network-based inverse dynamic model was used as a feed-forward gain.

Su et al. [24] used a neural network-based controller for a single-link flexible manipulator. They developed two separate neural networks with an adaption mechanism to compensate for the nonlinearities and friction. Finally they used a linear control scheme to control the flexible manipulator. Some other

research that has been done on controlling flexible link manipulators with the help of neural networks are listed in the following references [25-30].

Lin et al [31] developed a high-performance deep neural network to compensate for gravity and external disturbances. For the gravity compensation, a feed-forward neural network was trained based on the dynamics of the system. Whereas for the modeling of the external disturbances, 2 different scenarios were considered: configuration-dependent disturbances, and direction-dependent disturbances. A big neural network was developed for rejecting the disturbances. The knowledge distillation technique was used to condense the large neural network for real-time implementation.

Mukhopadhyay et al. [32] modeled a robot's dynamic using a neural network. They used the robot's sensor data for training recurrent neural networks. They also presented a comparative study between three different types of recurrent neural networks ((Simple Recurrent Neural Network (SRNN), Long Short Term Memory (LSTM), and Gated Recurrent Unit (GRU)) and discussed different aspects of selecting the appropriate Recurrent Neural Network for dynamic modeling. Liu et al [33] used LSTM to develop the robot inverse dynamics model. Step input function was used as the input trajectories and Newton Euler's analytical model was used for calculating the output torque. Input and output data were paired together to train the developed neural network.

Liang et al. [34] modeled robot dynamics by trained deep learning neural networks using real-time physical data. They applied physical stimulation to the robot and used input-output data set for online training.

Panwar et al. [35] used a neural network for generating human-like trajectories for the bipedal robot. To ensure the stability of the whole-body, upper body movement was considered.

Narendra et al. [36] showed that a neural network can be used to identify and control nonlinear dynamics. A multilayer recurrent neural network with a specific configuration can be used to identify and control the nonlinear dynamical system.

Polydoros et al. [37] developed a real-time deep learning network for robotic applications, which can learn from noisy data and can converge quickly. Simulation results showed the superiority of the algorithms.

Neural network has been widely used for developing robot adaptive controllers [38], [39], [40], [41], [42].

By analyzing the above-mentioned literature, it has been noticed that artificial intelligence and the neural network has been widely used for robot dynamic modeling and control application but the deep neural network-based hybrid dynamic controller is still out of focus, which provides an opportunity to contribute

to this field. The contribution of this article is to develop a deep learning-based robot controller for a seven degrees of freedom exoskeleton robot. They established a method to generate data for training the deep neural network using the analytical model. The stability analysis of the proposed controller is done and the robustness of the controller to parameters variation are shown with the help of ANOVA. A comparative study with different nonlinear controllers is presented.

The roadmap of the article is to develop a dynamic model of the human lower extremity exoskeleton robot, generate different sets of trajectories, create a computed torque controller to simulate the robot dynamics for different sets of trajectories and different users, run the simulation and save the input-output data for different scenarios, define deep neural network architecture, train it. Finally, make a hybrid controller by combining the developed deep neural network and the PD controller to control the robot. The role of the PD controller is to compensate for the prediction errors. The stability and robustness of the controller to parameter variation have been analyzed.

The whole article can be divided into 8 sections. Section 2 describes the dynamic modeling of the human lower extremity exoskeleton robot. Section 3 explains the computed torque control techniques. Section 4 shows dynamic modeling using deep neural networks, training, and validation. Section 5 presents the control algorithms based on the deep neural network and its stability analysis. Section 6 presents the simulation results using the developed controller. Section 7 presents the robustness analysis of the developed controller with the help of ANOVA and section 8 presents the comparative studies between the developed controller and the computed torque controller, sliding mode controller, adaptive controller, and the LQR controller.

## **2. Dynamic Modeling of the Exoskeleton Robot**

The modified DH parameter approach (Figure 2) was used to allocate link frames to individual degrees of freedom and the resultant DH parameter table (Table 1) was constructed. By substituting the value of the DH parameters in the general form of the homogeneous transformation matrix shown in Eqn. (1), the individual transformation matrix was found (Eqn. (2)-(8)). The complete forward kinematics was obtained by multiplying 7 transformation matrices together (Eqn. (9)). The forward kinematics specifies the end frame's position and orientation concerning the base frame.

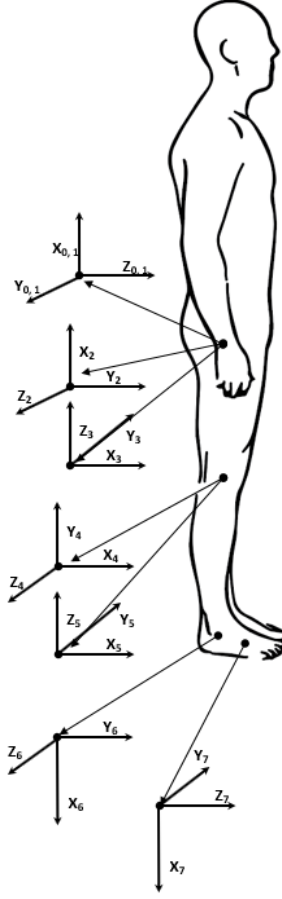


Figure 2 Link Frame assignment based on modified D-H parameter

Table 1: Human lower extremity DH parameters

Joint (i)	Joint name		Joint variable	Link offset	Link length	Link twist
			$\theta_i$	$d_i$	$a_{i-1}$	$\alpha_{i-1}$
1.	Abduction/Adduction		$\theta_1$	0	0	0
2.	Hip	Flexion/Extension	$\theta_2 - \frac{\pi}{2}$	0	0	$-\frac{\pi}{2}$
3.		Internal/External rotation	$\theta_3$	$-l_1$	0	$-\frac{\pi}{2}$
4.		Flexion/Extension	$\theta_4$	0	0	$\frac{\pi}{2}$
5.	Knee	Internal rotation	$\theta_5$	$-l_2$	0	$-\frac{\pi}{2}$
6.		Dorsiflexion/Plantarflexion	$\theta_6 - \frac{\pi}{2}$	0	0	$\frac{\pi}{2}$

$${}^i_{i-1}T = \begin{bmatrix} \cos\theta_i & -\sin\theta_i & 0 & \alpha_{i-1} \\ \sin\theta_i \cos\alpha_{i-1} & \cos\theta_i \cos\alpha_{i-1} & -\sin\alpha_{i-1} & -\sin\alpha_{i-1} d_i \\ \sin\theta_i \sin\alpha_{i-1} & \cos\theta_i \sin\alpha_{i-1} & \cos\alpha_{i-1} & \cos\alpha_{i-1} d_i \\ 0 & 0 & 0 & 1 \end{bmatrix} \quad (1)$$

$${}^0T_1 = \begin{bmatrix} \cos(\theta_1) & -\sin(\theta_1) & 0 & 0 \\ \sin(\theta_1) & \cos(\theta_1) & 0 & 0 \\ 0 & 0 & 1 & 0 \\ 0 & 0 & 0 & 1 \end{bmatrix} \quad (2)$$

$${}^1T_2 = \begin{bmatrix} \sin(\theta_2) & \cos(\theta_2) & 0 & 0 \\ 0 & 0 & 0 & 0 \\ \cos(\theta_2) & -\sin(\theta_2) & 1 & 0 \\ 0 & 0 & 0 & 1 \end{bmatrix} \quad (3)$$

$${}^2T_3 = \begin{bmatrix} \cos(\theta_3) & -\sin(\theta_3) & 0 & 0 \\ 0 & 0 & 0 & -l_1 \\ -\sin(\theta_3) & -\cos(\theta_3) & 1 & 0 \\ 0 & 0 & 0 & 1 \end{bmatrix} \quad (4)$$

$${}^3T_4 = \begin{bmatrix} \cos(\theta_4) & -\sin(\theta_4) & 0 & 0 \\ 0 & 0 & -1 & 0 \\ \sin(\theta_4) & \cos(\theta_4) & 0 & 0 \\ 0 & 0 & 0 & 1 \end{bmatrix} \quad (5)$$

$${}^4T_5 = \begin{bmatrix} \cos(\theta_5) & -\sin(\theta_5) & 0 & 0 \\ 0 & 0 & 1 & -l_2 \\ -\sin(\theta_5) & -\cos(\theta_5) & 0 & 0 \\ 0 & 0 & 0 & 1 \end{bmatrix} \quad (6)$$

$${}^5T_6 = \begin{bmatrix} \sin(\theta_6) & \cos(\theta_6) & 0 & 0 \\ 0 & 0 & -1 & 0 \\ -\cos(\theta_6) & \sin(\theta_6) & 0 & 0 \\ 0 & 0 & 0 & 1 \end{bmatrix} \quad (7)$$

$${}^6T_7 = \begin{bmatrix} \cos(\theta_7) & -\sin(\theta_7) & 0 & a_1 \\ 0 & 0 & 1 & 0 \\ -\sin(\theta_7) & -\cos(\theta_7) & 0 & 0 \\ 0 & 0 & 0 & 1 \end{bmatrix} \quad (8)$$

$${}^0_7T = [{}^0_1T \ {}^1_2T \ {}^2_3T \ {}^3_4T \ {}^4_5T \ {}^5_6T \ {}^6_7T] \quad (9)$$

Lagrange's energy method is a compelling technique to capture the dynamics of a rigid body. At any given moment the potential energy of a rigid body depends on its position Eqn. (10)-(11) and the kinetic energy of the rigid body depends on the velocity Eqn. (12)-(13). After calculating the total energy, based on the Lagrange method (equation (14)) the dynamic equation of motion was developed.

$$u_i = -m_i \cdot {}^0g^T \cdot {}^0P_{ci} + u_{ref} \quad (10)$$



$$u = \sum_{i=1}^n u_i \quad (11)$$

$$k_i = \left[ \frac{1}{2} m_i \cdot v_{ci}^T \cdot v_{ci} + \frac{1}{2} {}^i \omega_{ci}^T \cdot {}^{ci} I_i \cdot \omega_{ci} \right] \quad (12)$$

In Eqn. (10),  $m_i$  is the mass of the link,  $g$  is the gravitational acceleration, and  ${}^0P_{ci}$  is the location of the center of mass of the link with respect to the reference ground. In Eqn. (11),  $n$  is the total number of links. In Eqn. (12),  $m_i$  present the mass of the link,  $v_{ci}$  and  $\omega_{ci}$  express the linear and angular velocity of the link at the link's center of mass and  $I_i$  is the link's moment of inertia at its center of mass.

$$k = \sum_{i=1}^n k_i \quad (13)$$

$$\tau_i = \left[ \frac{d}{dt} \frac{\delta k}{\delta \dot{\theta}_i} - \frac{\delta k}{\delta \theta_i} + \frac{\delta u}{\delta \theta_i} \right] \quad (14)$$

The anthropometric parameters that were used for developing robot dynamics equation of motion are given in Eqn. (15)-(35),

$$B_d = 0.6905 + 0.0297C \frac{lb}{ft^3}, \text{ where } C = HW^{-\frac{1}{3}}, \quad (15)$$

In Equation (15),  $B_d$  is the body density ( $lbs/ft^3$ ),  $H$  is the height of the subject ( $inch$ ),  $W$  is the body weight of the subject ( $lbs$ ). Thigh, shank and foot densities determined by the following equations,

$$T_d = 1.035 + 0.814 * B_d \frac{lb}{ft^3} \quad (16)$$

$$S_d = 1.065 + B_d \frac{lb}{ft^3} \quad (17)$$

$$F_d = 1.071 + B_d \frac{lb}{ft^3} \quad (18)$$

In Eqns. (16)-(18),  $T_d$  is the thigh density,  $S_d$  is the shank density and  $F_d$  is the foot density. The whole body volume ( $B_v$ ) was calculated using body weight and body density,

$$B_v = \frac{W}{B_d} ft^3 \quad (19)$$

The volume of thigh, shank and foot were calculated as follows:

$$T_v = 0.0922 * B_v ft^3 \quad (20)$$

$$S_v = 0.0464 * B_v ft^3 \quad (21)$$

$$F_v = 0.0124 * B_v ft^3 \quad (22)$$

The weights of the thigh, shank and foot were calculated by the Eqns. (23)-(25)

$$T_m = T_v * T_d \text{ lbs} \quad (23)$$

$$S_m = S_v * S_d \text{ lbs} \quad (24)$$

$$F_m = F_v * F_d \text{ lbs} \quad (25)$$

The length of the thigh ( $T_l$ ), shank ( $S_l$ ), foot ( $F_l$ ) and ankle to the lower face of the foot ( $A_g$ ) were calculated by Eqns. (26)-(29),

$$T_l = 0.245 * H \text{ inch}, \quad (26)$$

$$S_l = 0.285 * H \text{ inch}, \quad (27)$$

$$F_l = 0.152 * H \text{ inch}, \quad (28)$$

$$A_g = 0.043 * H \text{ inch} \quad (29)$$

The locations of the center of the mass from the proximal joint (for thigh ( $T_{cm}$ ), shank ( $S_{cm}$ ), foot ( $F_{cm}$ )) are given by Eqns. (30)-(32)

$$T_{cm} = 0.41 * T_l \text{ inch}, \quad (30)$$

$$S_{cm} = 0.393 * S_l \text{ inch}, \quad (31)$$

$$F_{cm} = 0.445 * F_l \text{ inch} \quad (32)$$

The empirical equations for the inertial properties of the thigh  $T_i$ , shank  $S_i$ , and foot  $F_i$  are given in Eqns (33) - (35),

$$T_i = \begin{bmatrix} T_m (0.124 * T_l)^2 & 0 & 0 \\ 0 & T_m (0.267 * T_l)^2 & 0 \\ 0 & 0 & T_m (0.267 * T_l)^2 \end{bmatrix} \quad (33)$$

$$S_i = \begin{bmatrix} S_m (0.281 * S_l)^2 & 0 & 0 \\ 0 & S_m (0.114 * S_l)^2 & 0 \\ 0 & 0 & S_m (0.275 * S_l)^2 \end{bmatrix} \quad (34)$$

$$F_i = \begin{bmatrix} F_m (0.124 * F_l)^2 & 0 & 0 \\ 0 & F_m (0.245 * F_l)^2 & 0 \\ 0 & 0 & F_m (0.257 * F_l)^2 \end{bmatrix} \quad (35)$$

Eqn. (15)-(35) were incorporated into the dynamic equation of motion of the robot.

The robot's dynamic equation of motion ((14) can be rewritten as Eqn. (36),

$$\tau_{Joint} = [M(\theta)\ddot{\theta} + V(\theta, \dot{\theta}) + G(\theta)] \quad (36)$$

In Eqn. (36),  $M(\theta)$  is the mass matrix which is a (7x7) symmetric positive definite matrix,  $V(\theta, \dot{\theta})$ , (7x1) is the Coriolis and the centripetal term, and the gravitational term is represented by  $G(\theta)$ ,

$(7 \times 1)$  matrix.  $\tau_{Joint}$ ,  $(7 \times 1)$  presents the joints torque requirements. The robot dynamic equation of motion can be written as,

$$\ddot{\theta} = M(\theta)^{-1}(\tau_{Joint} - V(\theta, \dot{\theta}) - G(\theta)) \quad (37)$$

Figure 3 shows the architecture of an ideal robot dynamics (without joints friction).

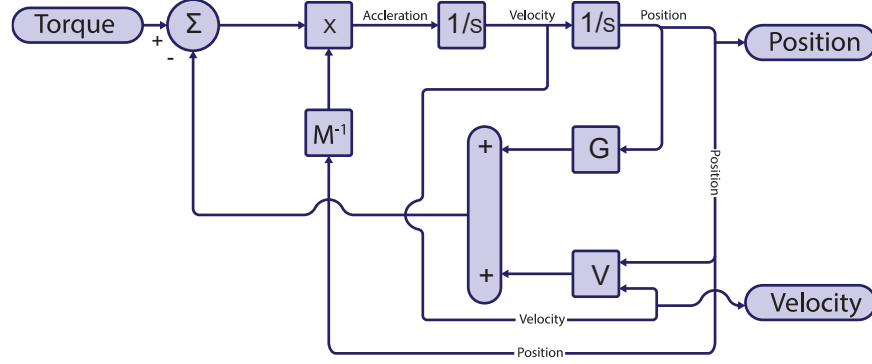


Figure 3 Internal architecture of the robot model

Naturally friction is induced between two mechanical mating parts with relative motion. The robot dynamics grow more complex by incorporating joint friction torques.

$$\tau_{Joint} = [M(\theta)\ddot{\theta} + V(\theta, \dot{\theta}) + G(\theta) + \tau_{friction}] \quad (38)$$

Where,

$$\tau_{friction} = [f(\dot{\theta})] \quad (39)$$

Eqn. (37) can be rewritten as Eqn. (40)

$$\ddot{\theta} = M(\theta)^{-1}(\tau_{Joint} - V(\theta, \dot{\theta}) - G(\theta) - f(\dot{\theta})) \quad (40)$$

The robot dynamics with frictional disturbances are schematically depicted in Figure 4

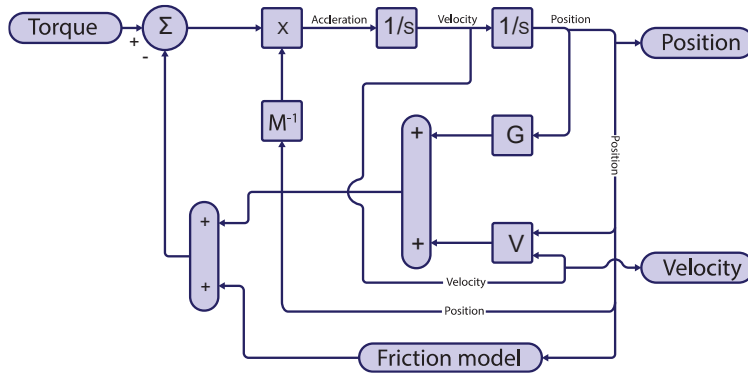


Figure 4 Internal architecture of the physical Robot model

The used friction model combined the Coulomb friction, the Viscous friction, and the Stribeck effect [43].

The Eqn. (41) to Eqn. (43) approximate the joint friction torques:

$$T = \sqrt{(2e)}(T_{brk} - T_C) \cdot \exp\left(-\left(\frac{\omega}{\omega_{St}}\right)^2\right) \cdot \frac{\omega}{\omega_{St}} + T_C \cdot \tanh\left(\frac{\omega}{\omega_{Coul}}\right) + f\omega \quad (41)$$

$$\omega_{St} = \omega_{brk}\sqrt{2} \quad (42)$$

$$\omega_{Coul} = \frac{\omega_{brk}}{10} \quad (43)$$

Where,

$T$  represents the total friction

$T_C$  represents the Coulomb friction

$T_{brk}$  represents the breakaway friction torque: The Breakaway friction is defined as the sum of the Coulomb and Stribeck frictions in the vicinity of zero velocity.

$\omega_{brk}$  represents the breakaway friction velocity: The velocity at which the Stribeck friction is at its peak. At this point, the sum of the Stribeck and Coulomb friction is the Breakaway friction force.

$\omega_{St}$  represents the Stribeck velocity threshold

$\omega_{Coul}$  represents the Coulomb velocity threshold

$\omega$  represents the input angular velocity

$f$  is the coefficient of viscous friction: The coefficient of proportionality between the friction torque and the angular velocity. The parameter must have a positive value.

The simulated friction model is shown in Figure 5.

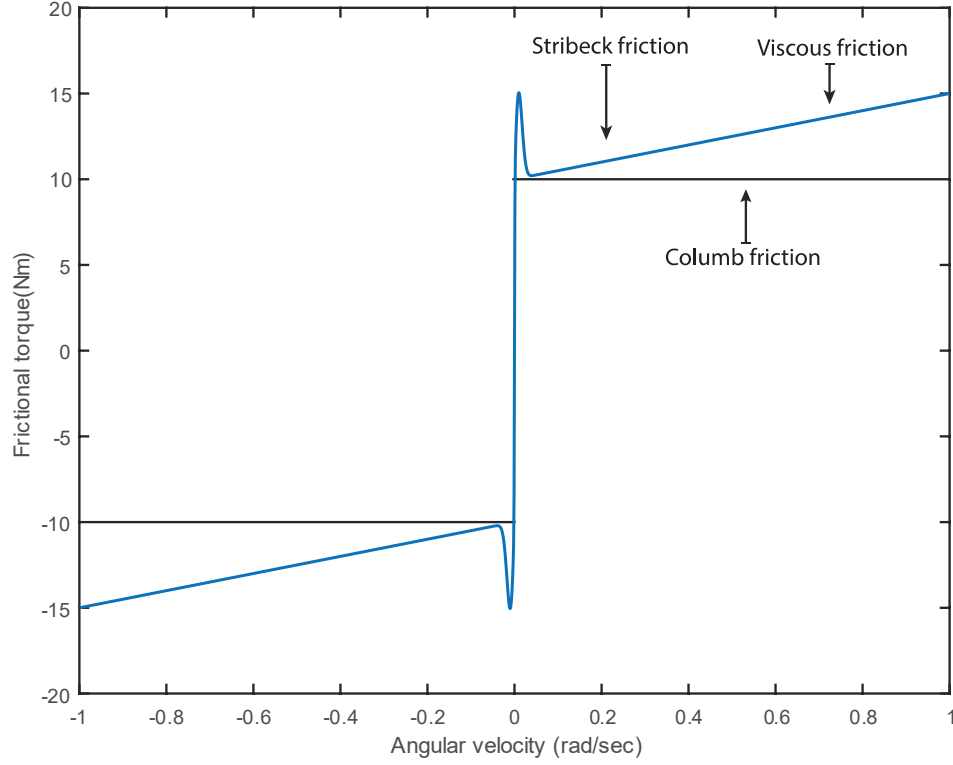


Figure 5 Friction model simulation

The parameters used for friction simulation are given below,

$$T_{Peak} = 100 \text{ Nm}, \omega = 100 \text{ rad/sec}, f = 5 \text{ Nm/(rad/sec)}, T_{Columb} = 0.1 * T_{Peak} \text{ Nm},$$

$$\omega_{brk} = 0.01 \text{ rad/sec}, T_{brk} = 0.15 * T_{Peak} \text{ Nm}$$

### 3. Computed Torque control

The computed torque control scheme calculates robot joints' trajectory tracking torque requirements by using robot inverse dynamics. The computed torque control system accomplishes two goals: Linearize the nonlinear robot dynamics by providing the required torque to mitigate the effects of gravity and Coriolis-centrifugal force (Figure 6, linearization loop) and to provide the controlled torque to track the robot input trajectories (Figure 6, control loop).

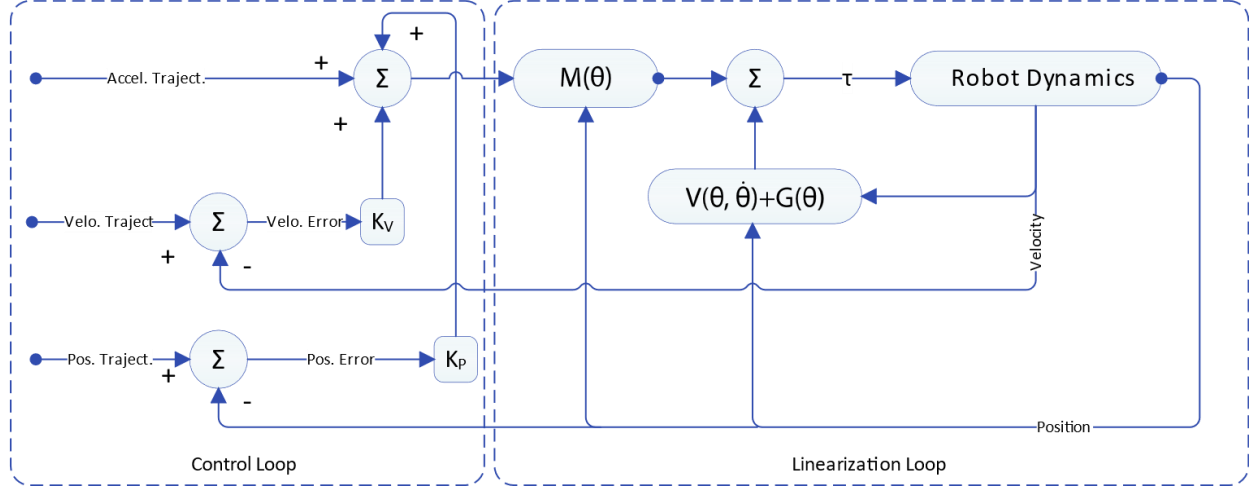


Figure 6 Computed torque control scheme

An accurate dynamic model is required for designing and implementing the computed torque controller. Most of the time, constructing an accurate dynamic model is impractical. That's a main drawback of computed torque controller.

According to the computed torque control scheme, the input torque to the robot is given by Eq. (44),

$$\tau = M(\theta) [\ddot{\theta}_d + K_v(\dot{\theta}_d - \dot{\theta}) + K_p(\theta_d - \theta)] + V(\theta, \dot{\theta}) + G(\theta) \quad (44)$$

In Eqn. (44),  $\theta_d$ ,  $\dot{\theta}_d$  and  $\ddot{\theta}_d$  presents the robot's desired trajectories. The real position velocity and acceleration of the robot are represented by  $\theta$ ,  $\dot{\theta}$  and  $\ddot{\theta}$ .  $K_p, K_v$  are the positive definite gain matrices.  $M(\theta)$  presents the robot mass matrix,  $V(\theta, \dot{\theta})$  presents the Coriolis and centrifugal force and  $G(\theta)$  is the gravitational term of the robot dynamics.

#### 4. Dynamic modeling using Deep Neural Network

A neural network is a collection of interconnected neurons. In a feedforward neural network, no feedback mechanism is employed. A deep neural network consists of multiple hidden layers. Figure 7 presents the architecture of the developed deep-feed forward neural network [44]. The constructed deep feed-forward neural network uses a total of 49 ( $21 \times 14 \times 7 \times 7$ ) neurons (Figure 8), that are distributed in three hidden layers and one output layer. A total of 224 numbers of weight elements (including neuron biases and weights) were used. Tan-Sigmoid transfer functions (tan hyperbolic) were used in the hidden layers, while the Linear transfer functions (pure linear) were used in the output layer. During the construction of the neural network, a couple of transfer functions were tested, Tan-Sigmoid transfer function gave better performance than others. It has been noticed that even adding an extra neuron in any layer or adding a

new layer leads to overfitting. One of the main goals in developing the structure of the deep neural network was to keep it as small as possible to reduce the physical controller's computational load.

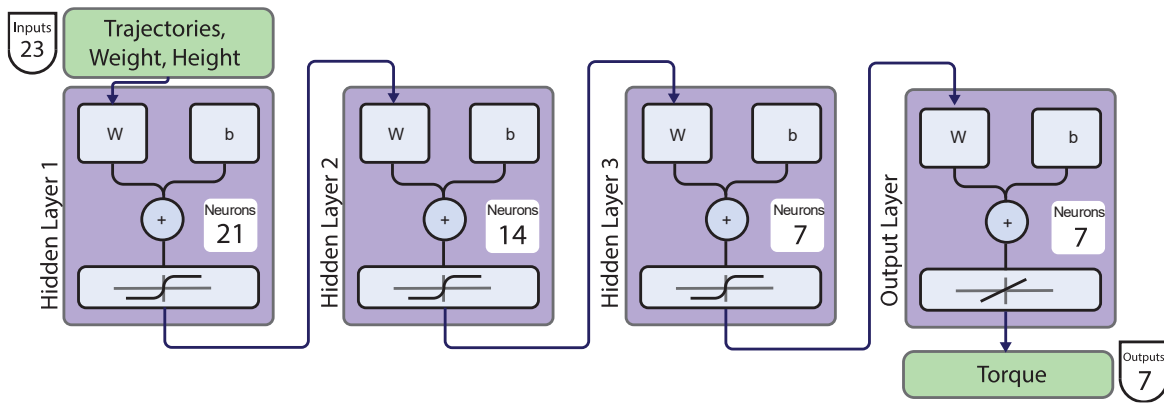


Figure 7 Architecture of the developed neural network

For training the developed neural network, two sets of data were produced. The first set was for the sequential joint movements: when seven joints moved one after another, and the second set was for the simultaneous joint movements: when all the joints started moving together. Training Data were produced by hierarchical combinations of robot joint positions, velocities and accelerations, and subjects' height and weight. Figure 9 presents the training data generation hierarchy.

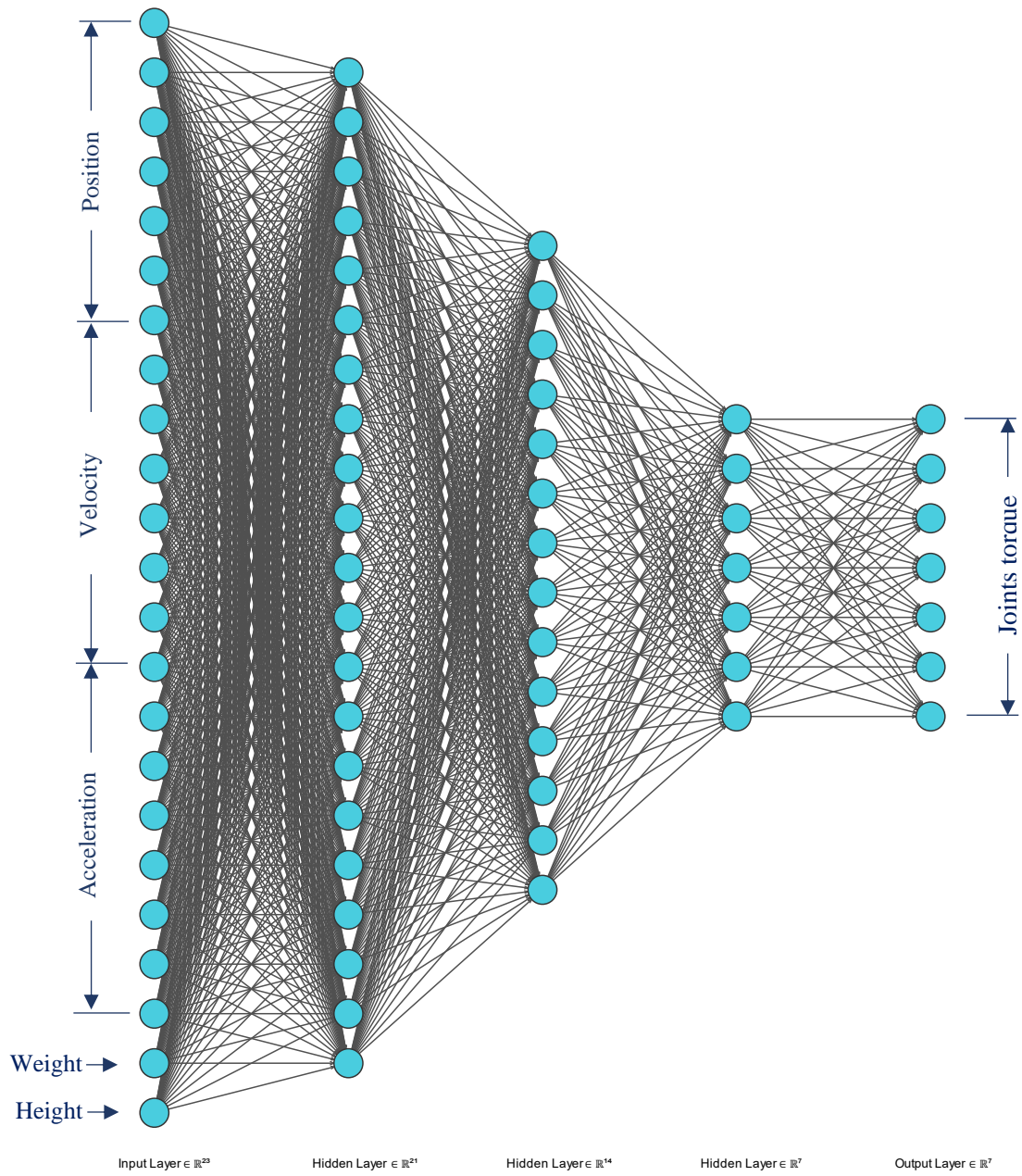


Figure 8 Developed deep neural network for joint torque estimation



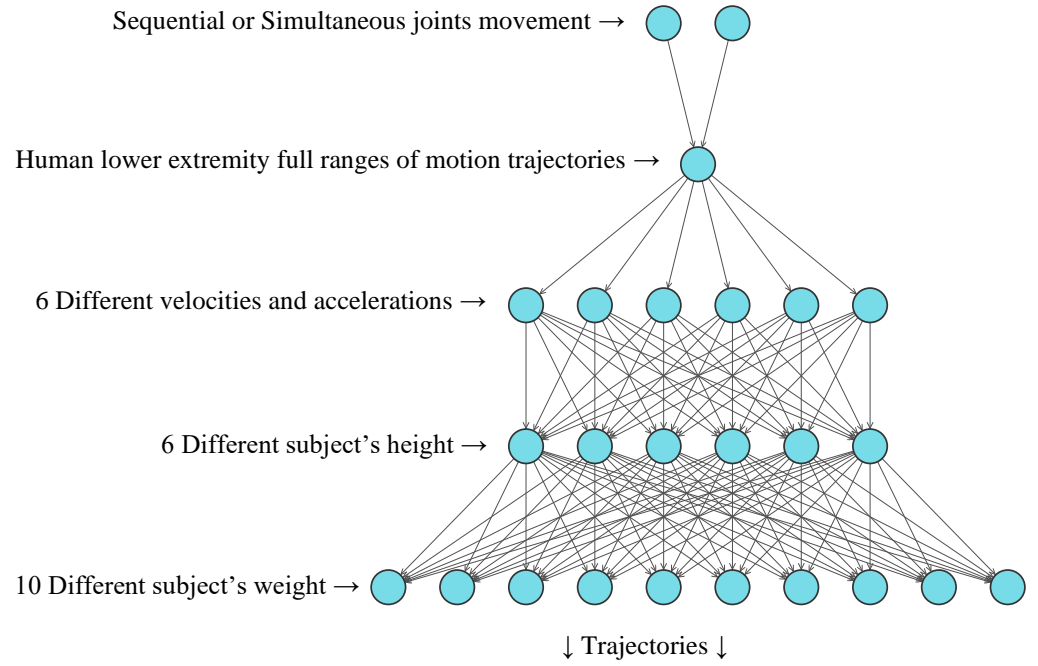


Figure 9 Hierarchical data generation schematic diagram

Seven joint positions, velocities, accelerations, subject's weight, and height obtained from different combinations were used as input to the computed torque controller-based dynamic simulation, and the output of the computed torque controller (7 joints torques) were saved for the training purpose. Figure 10 shows the schematics diagram of the computed torque controller-based dynamic simulation. The purple color highlighted the input of the simulation and the green color presented the outputs.

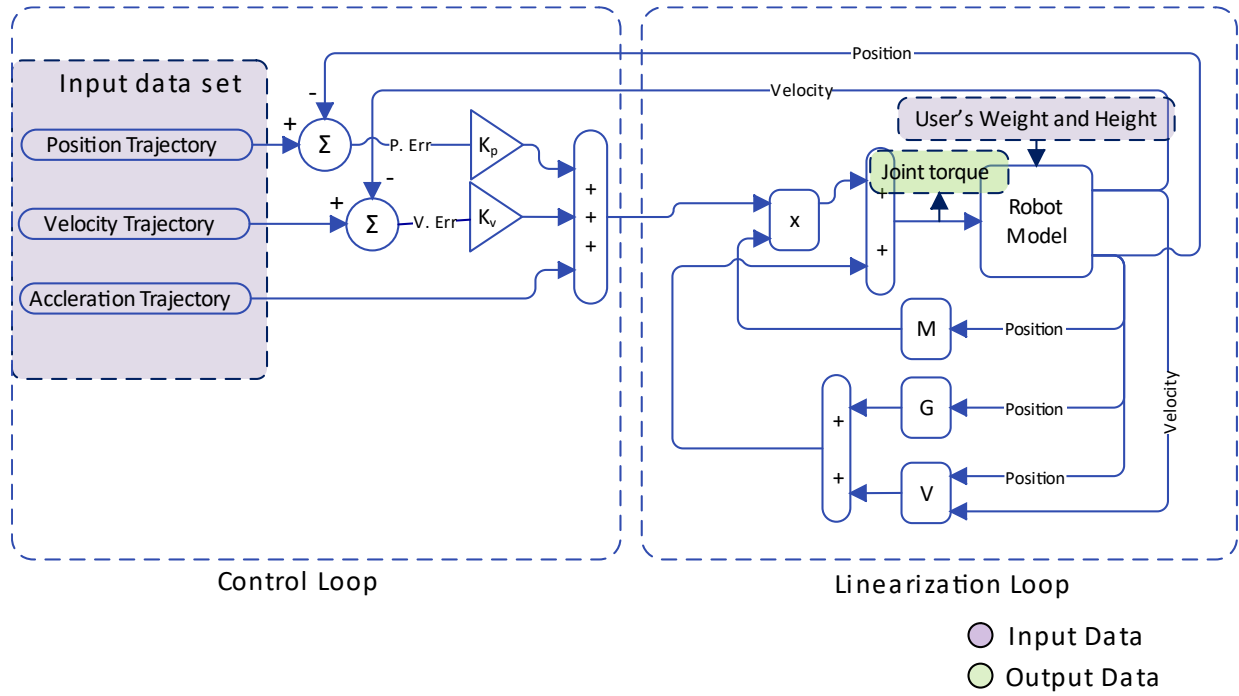


Figure 10 Input and Output data tracing locations in the simulation

Simulations were run for both sequential joint movements and simultaneous joint movements. A total of 43560880 sets of data were produced. Available data were down-sampled by a factor of 10 to reduce the data size. Correlation analyses of the data were performed to select the important features and reduce the input size. It has been noticed that input trajectories, weight, and height have a good correlation with the output torques, as a result, all inputs were considered. For the training, the neural network at a total of 4356088 sets of data was used. Each data set consists of 23 inputs (7 joints' desired positions, 7 joints' velocities, 7 joints' accelerations, user's height and weight) and 7 outputs (7 joints torques).

For the generation of the input data set, human lower extremity full ranges of motion were considered. Figure 11 presents the full ranges of motion trajectories. The left-side figure shows the simultaneous joint movements, and the right-side figure shows the sequential joint movements.

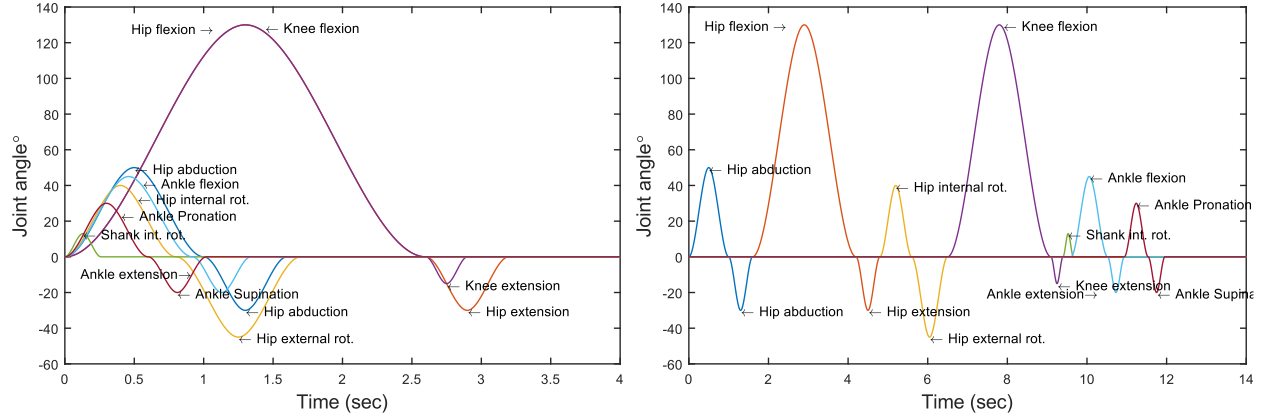


Figure 11 Simultaneous and sequential joint movements (constructed based on the human lower extremity's full ranges of motion [45])

For producing the deep neural network training data, the same position trajectories were run at different velocities with different subject's height and mass. Different velocities, subject's weight and height used for training data generation are given in Table 2.

Table 2 Different values of joints velocities, subject's weight and height used for input data generation

Joints velocity	10, 20, 30, 40, 50, 60, 70, 80, 90, 100 [deg/sec]
Subject's height	50, 55, 60, 70, 75 [inch]
Subject's weight	150, 160, 170, 180, 190, 200, 210, 220, 230, 240, 250 [lbs.]

The key role of the developed deep neural network is to estimate the torque requirement based on the input trajectories and the subject's height and weight. For dynamic modeling, only the human lower extremity's anthropometric parameters were considered.

For training the developed neural network, Levenberg-Marquardt optimization algorithm was used. 70% of the total data were used for the network training, 15% for validation, and the remaining 15% used for testing. Training performances are quantified by the mean square error. Figure 12 presents the training, validation and testing performance of the developed neural network.

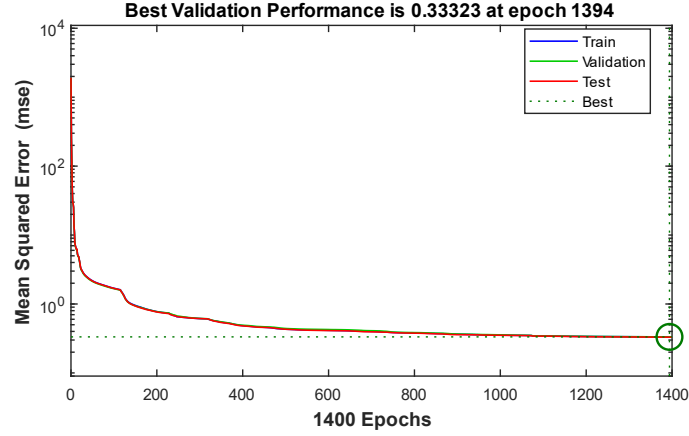


Figure 12 Training Neural network

### 5. Control algorithm based on the developed deep neural network model

The controller developed to maneuver the robot according to the input trajectories using the trained deep neural network is shown in Figure 13. Input trajectories, user's weight, and height were considered as the input of the trained deep neural network. Seven joint torques were predicted by the deep neural network. The developed deep neural network acts as the feed-forward gain to the controller. While designing the neural network it has been tried to use a minimum number of neurons. A PD controller was used inside the feedback loop to compensate for the prediction errors. The proportional gains ( $K_P$ ) were used for all joints of the PD controller 3000 and the derivative gains ( $K_V$ ) were 250.

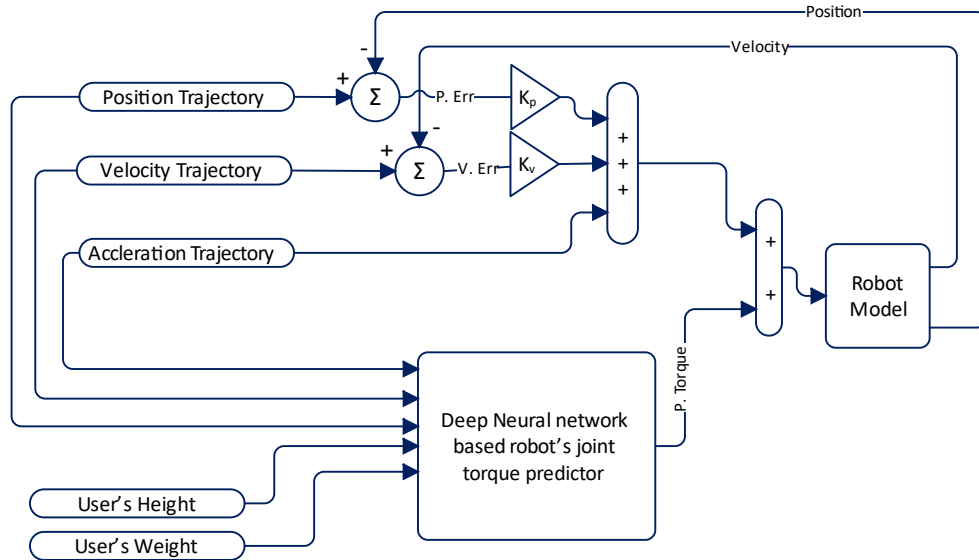


Figure 13 Control architecture of the Deep neural network-based robot controller

If the developed deep neural network can predict the joint's torque accurately the complicated nonlinear robot dynamics become linear and linear control techniques can be applied. The proposed deep neural network acts as the feed-forward controller. The PD controller was employed to remove the prediction errors. If the system is linearized closely, the stability of the system depends solely on the PD controller. A large amount of prediction error may badly affect the controller's stability.

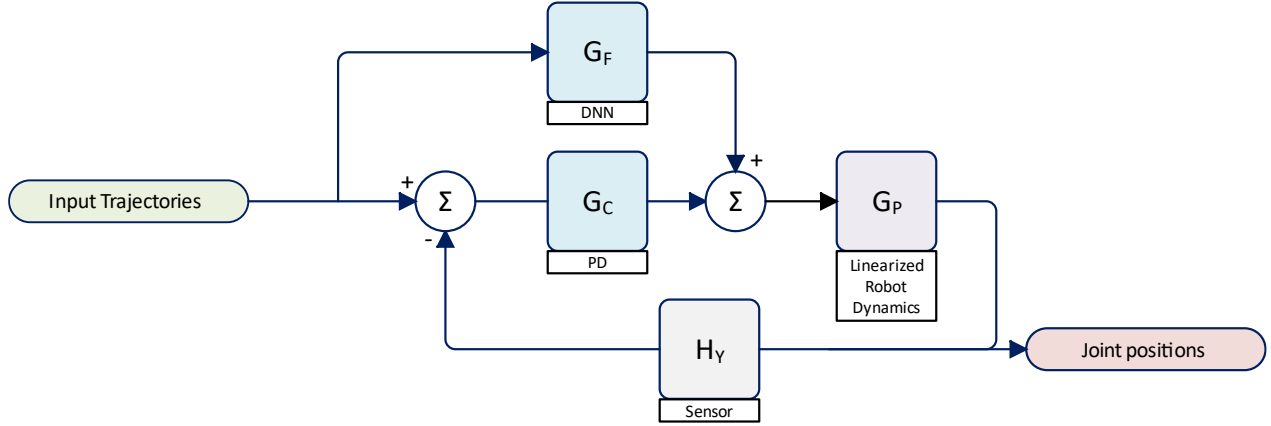


Figure 14 Architecture of the hybrid controller

The transfer function between the input trajectories and the joint positions can be presented by

$$\frac{\text{Joint position}}{\text{Input trajectories}} = \frac{G_P G_F (1 + G_C G_P H_Y) + G_C G_P}{1 + G_C G_P H_Y} \quad (45)$$

In Eqn. (45) The characteristics equation is given by,  $1 + G_C G_P H_Y = 0$ . The stability of the developed controller does not depend on the feed forward gain  $G_F$  provided by the deep neural network. The feed forward gain either amplifies or attenuates the output signal. If the deep neural network can predict accurately, the stability depends only on the PD controller gains.

## 6. Simulation results analysis

Figure 15 to Figure 20 presents the trajectory tracking performances of the developed deep neural network-based controller in simultaneous joint movements. Figure 15 shows the simultaneous trajectory tracking performance of all seven joints and Figure 16 shows the trajectory tracking errors. The maximum amount of observed trajectory tracking errors were  $[0.26^\circ, 0.20^\circ, 0.20^\circ, 0.26^\circ, -0.14^\circ, -0.21^\circ, 0.19^\circ]$ . From the simulation results, it has been shown that joint 4 experienced the maximum amount of trajectory tracking error ( $0.26^\circ$ ) followed by joint 1 and joint 6.

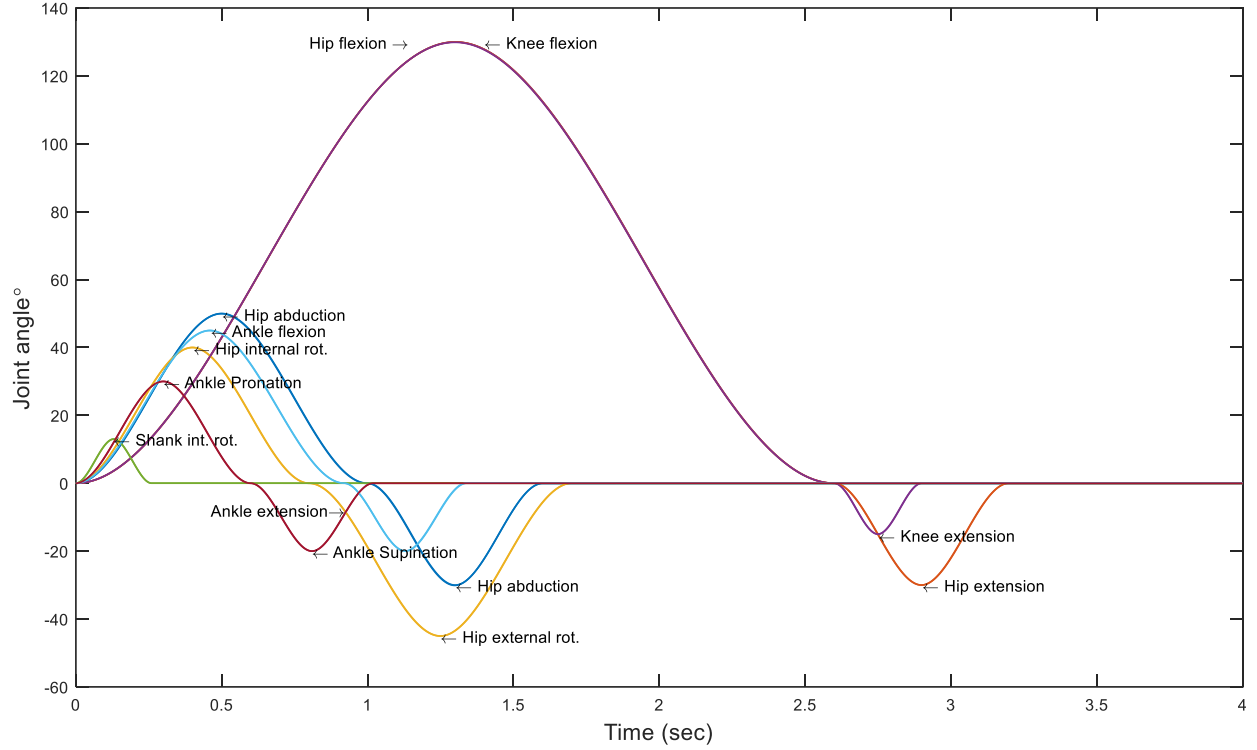


Figure 15 Trajectory tracking performance (Simultaneous joint movement)

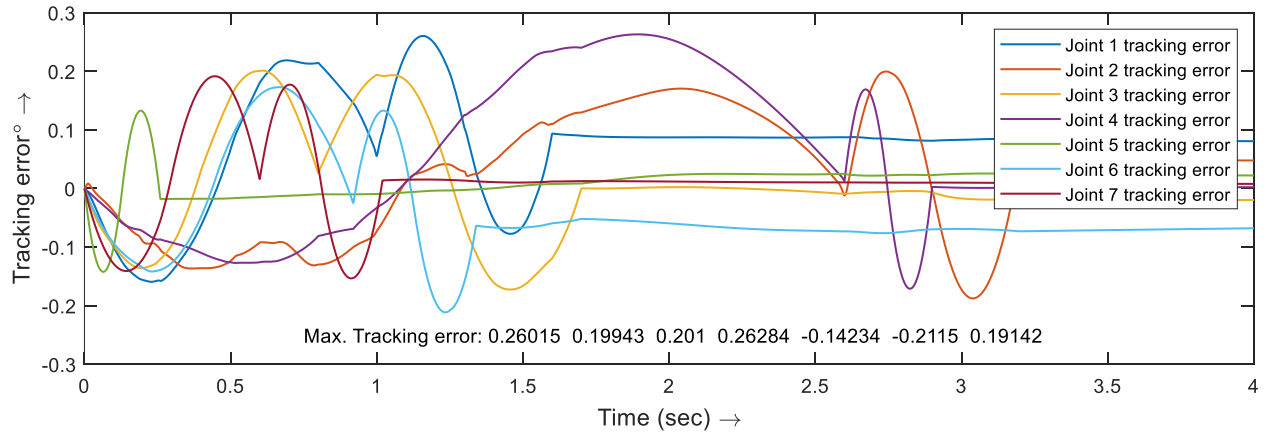


Figure 16 Trajectory tracking Error (Simultaneous joint movement)

Figure 17 shows the joint torque requirement for tracking the trajectories shown in Figure 15. The left column of Figure 17 shows the total amount of torque required for simultaneous trajectory tracking. The middle column of Figure 17 shows the deep neural network-based predicted joints torques and the right shows the contribution of the PD controller.

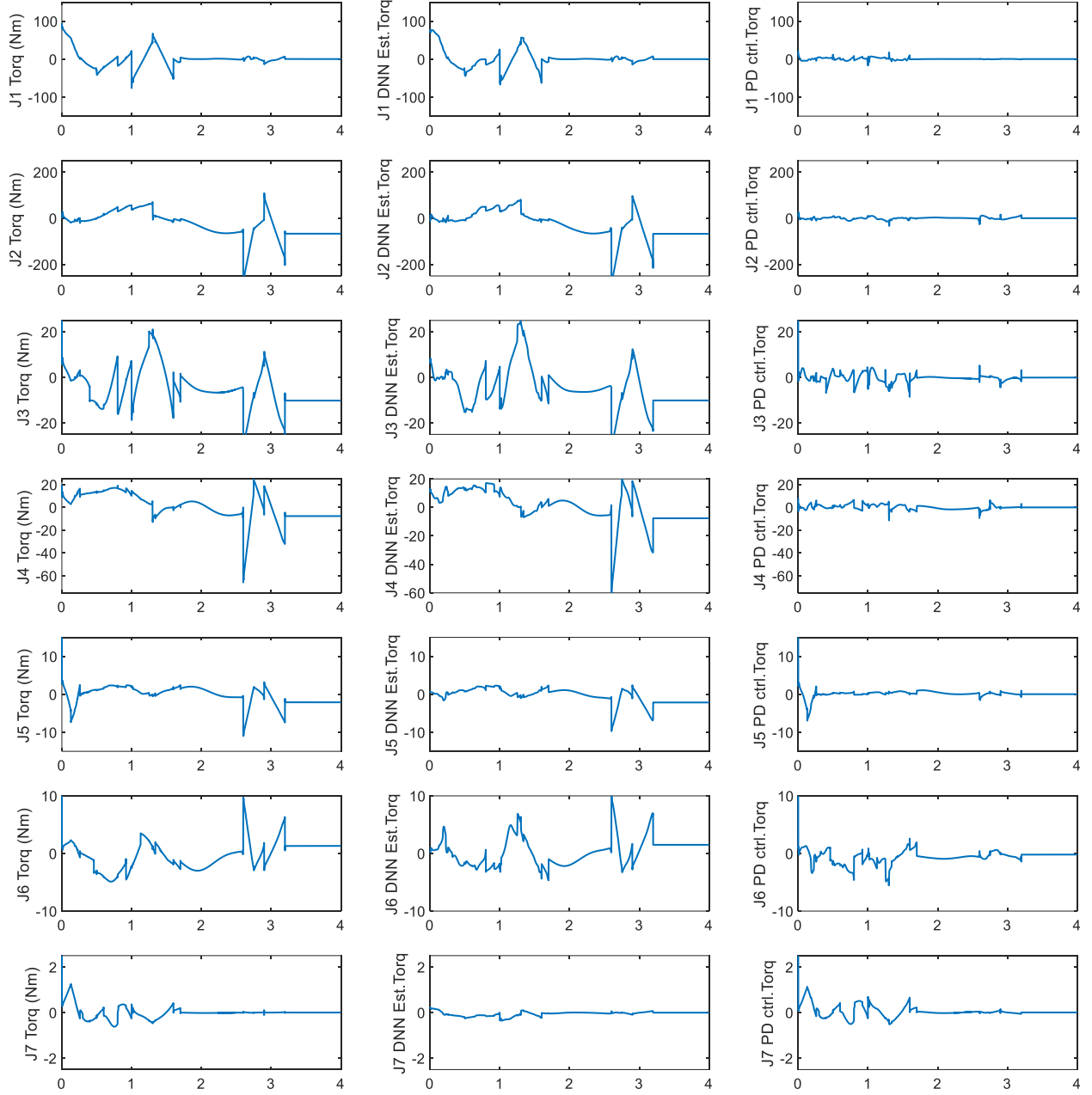


Figure 17 From the right: total Joint torque requirement for sequential joint movements, Predicted torque, PD controller's contribution

From Figure 17 it is visible that for the majority of the joints (joint 1 to joint 6) the predicted torque is very close to the amount of total required joint torque and the PD controller's contribution is very small. For the 7<sup>th</sup> joint the PD controller contributed little more than the predicted torque. As a deep neural network is considered a black-box model, it is very difficult to explain the inner mechanism. It was observed that the joint torque requirements for the seventh joint are much lower than other joints. Joint 7 dynamics was tried to capture by adding an extra neuron or an extra layer but adding an extra neuron or by adding an extra layer caused an overfitting problem.

Figure 18 shows the trajectory tracking performance of the developed deep neural network-based controller for sequential trajectory tracking. Figure 19 shows the trajectory tracking errors. The maximum amount of trajectory tracking errors was  $[-0.22^\circ, -0.26^\circ, -0.18^\circ, 0.25^\circ, -0.15^\circ, -0.19^\circ, -0.17^\circ]$ . Joint 2 experienced the maximum amount of trajectory tracking error ( $0.26^\circ$ ) followed by joint 4 and joint 1.

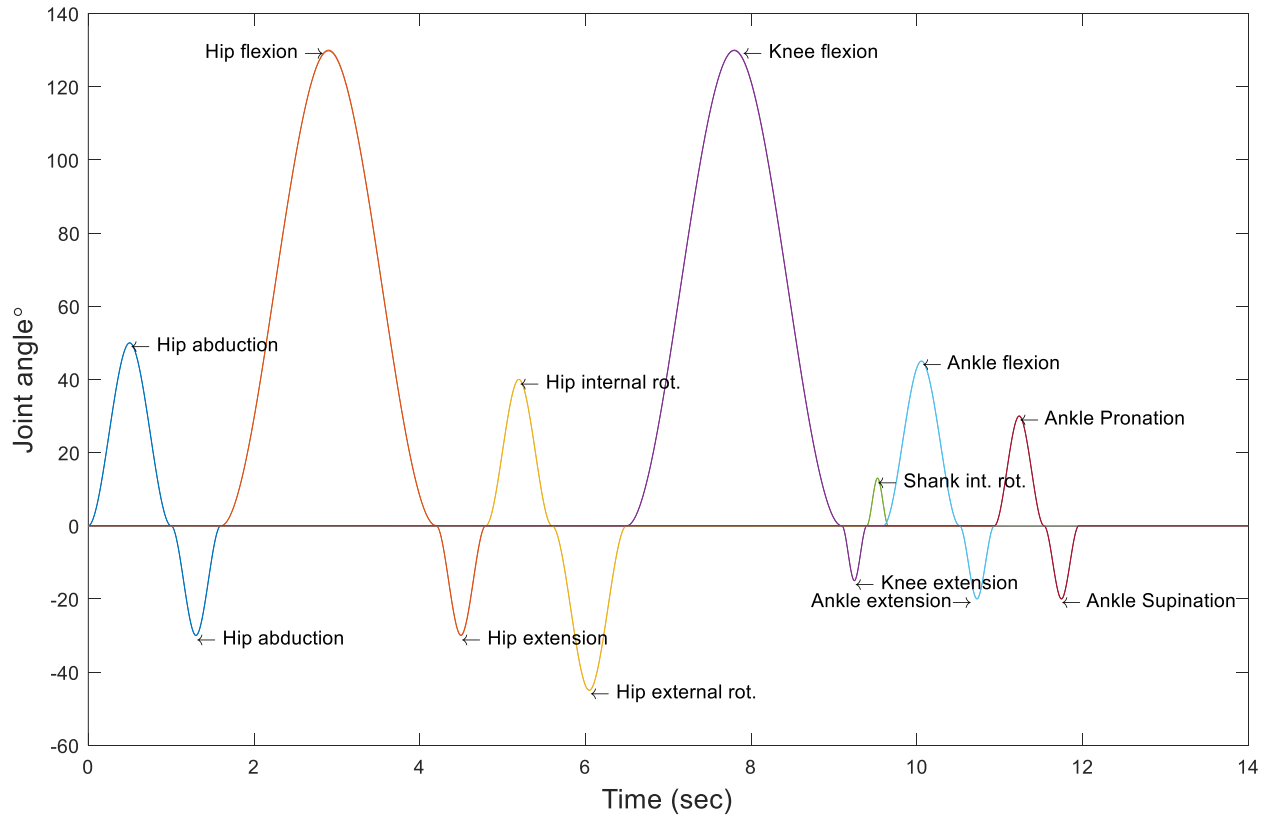


Figure 18 Trajectory tracking performance (Sequential joint movements)

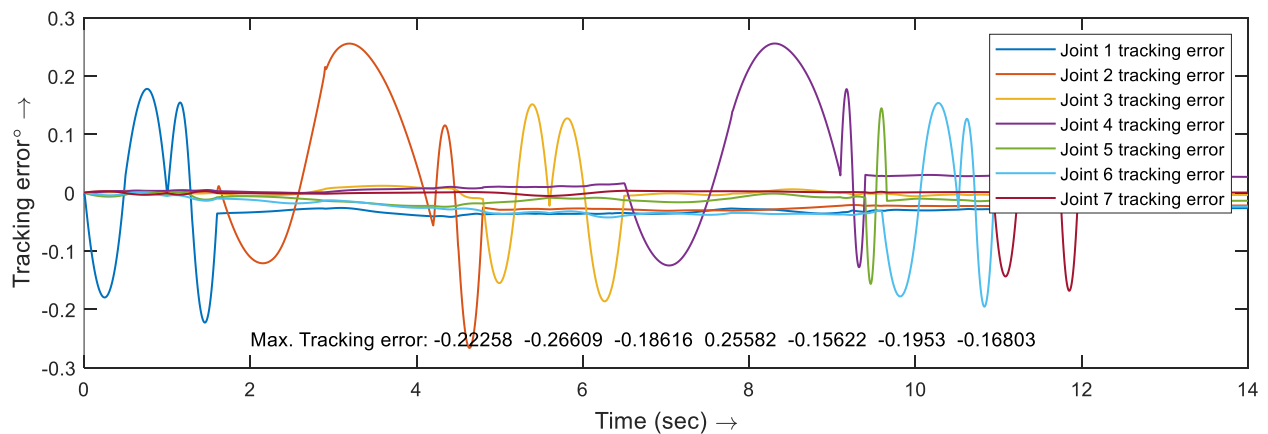


Figure 19 Trajectory tracking error (Sequential joint movements)



Figure 20 shows the joint torque distribution for the sequential trajectory tracking. In Figure 20 the left column shows the total joint torque required for tracking the sequential movements. The middle column of the Figure 20 presents the deep neural network-based predicted torques. And the right column presents the contribution of the PD controller. Like the simultaneous joint movements, the maximum amount of prediction errors was observed on joint 7. For joint 1 to joint 6 the deep neural network-based predicted torques were very close to the total joint torque requirements.

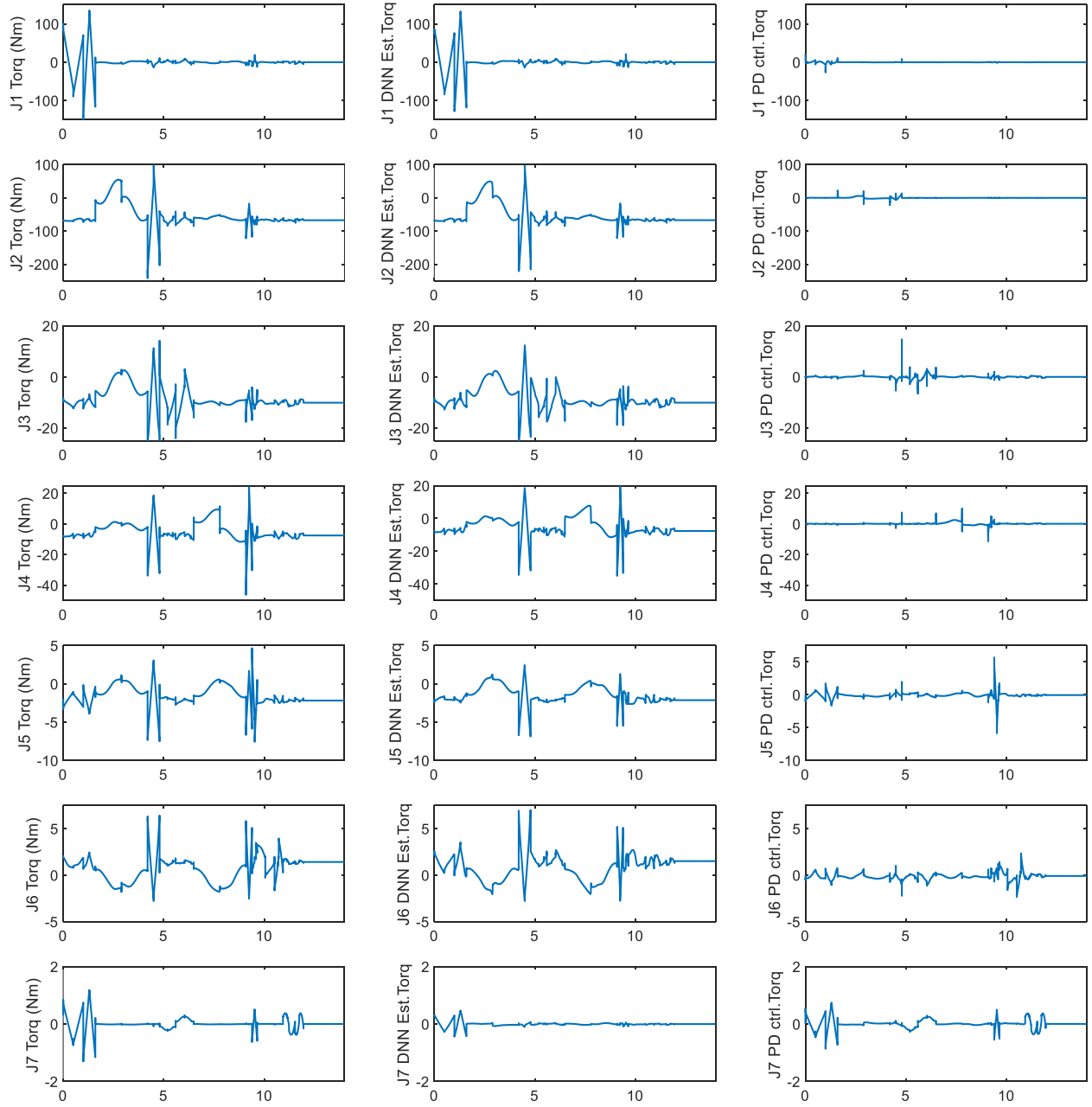


Figure 20 From the left: total Joint torque requirement for sequential joint movements, DNN Predicted torque, PD controller's contribution

It can be concluded that the trajectory tracking performance of the developed deep neural network-based controller is very high. The next section will present the robustness of the developed controller to the parameter variations.

## 7. Controller robustness analysis against parameter variations ANOVA

ANOVA is a statistical technique for determining the effects of system parameter variations. ANOVA was first introduced by Ronald Fisher in 1918 [46]. To evaluate the robustness of the designed controller the user's mass and length were varied, and the effects on the tracking errors were observed.

Statistically,  $P$  (measures the evidence against the null hypothesis) value plays a significant role. Any value of  $P < \textit{significance level}$  (0.005) expresses that at least one observation is affected by the change of the parameter. This experiment expressed the relation between tracking error and the user's mass or height. The one-way ANOVA test is applicable for only normally distributed data, and the sample size needs to be big enough for better performances. Figure 21 and Figure 22 show the tracking error distribution against the change of user's weight and height respectively, it is evident from the figures that all the tracking errors are normally distributed. The  $P$  values of all 7 joints are significantly higher than the significance level (0.005), (Table 3, Table 4) which concludes that the system is not affected by the changes in weight or height.

The complete form of the variables used in Table 3 and Table 4 are as follows,

**$SS$**  Sum of squares

**$df$**  - Degrees of freedom

**$MS$**  - Mean square

**$F$**  - statistic

**$Prob$**  - p-value

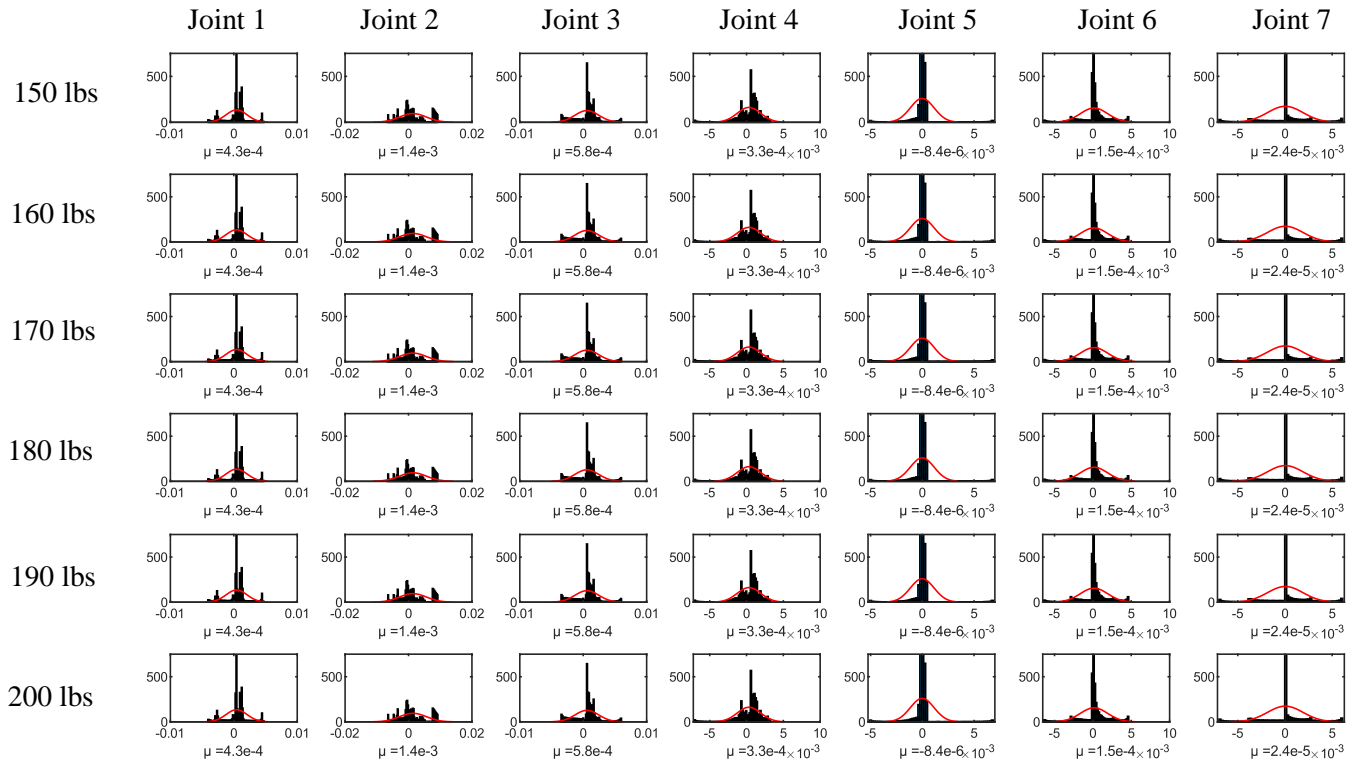


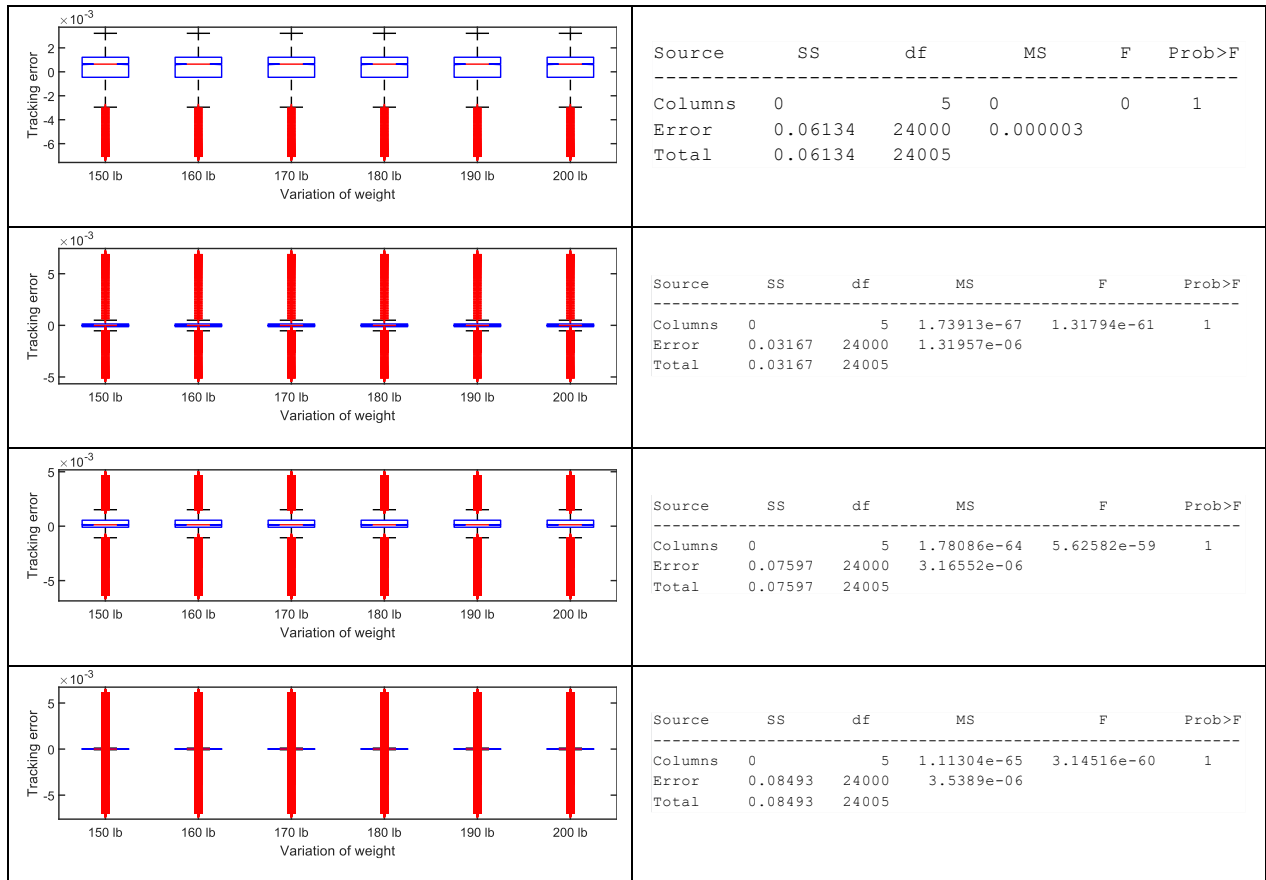
Figure 21 Tracking error distribution concerning weight variation

Table 3 Tracking error variation concerning the user's weight

Source	SS	df	MS	F	Prob>F
Columns	0	5	0	0	1
Error	0.06521	24000	0.000003		
Total	0.06521	24005			

Source	SS	df	MS	F	Prob>F
Columns	0	5	0	0	1
Error	0.43154	24000	0.000018		
Total	0.43154	24005			

Source	SS	df	MS	F	Prob>F
Columns	0	5	0	0	1
Error	0.08377	24000	0.000003		
Total	0.08377	24005			



Variation of tracking errors with subject's height

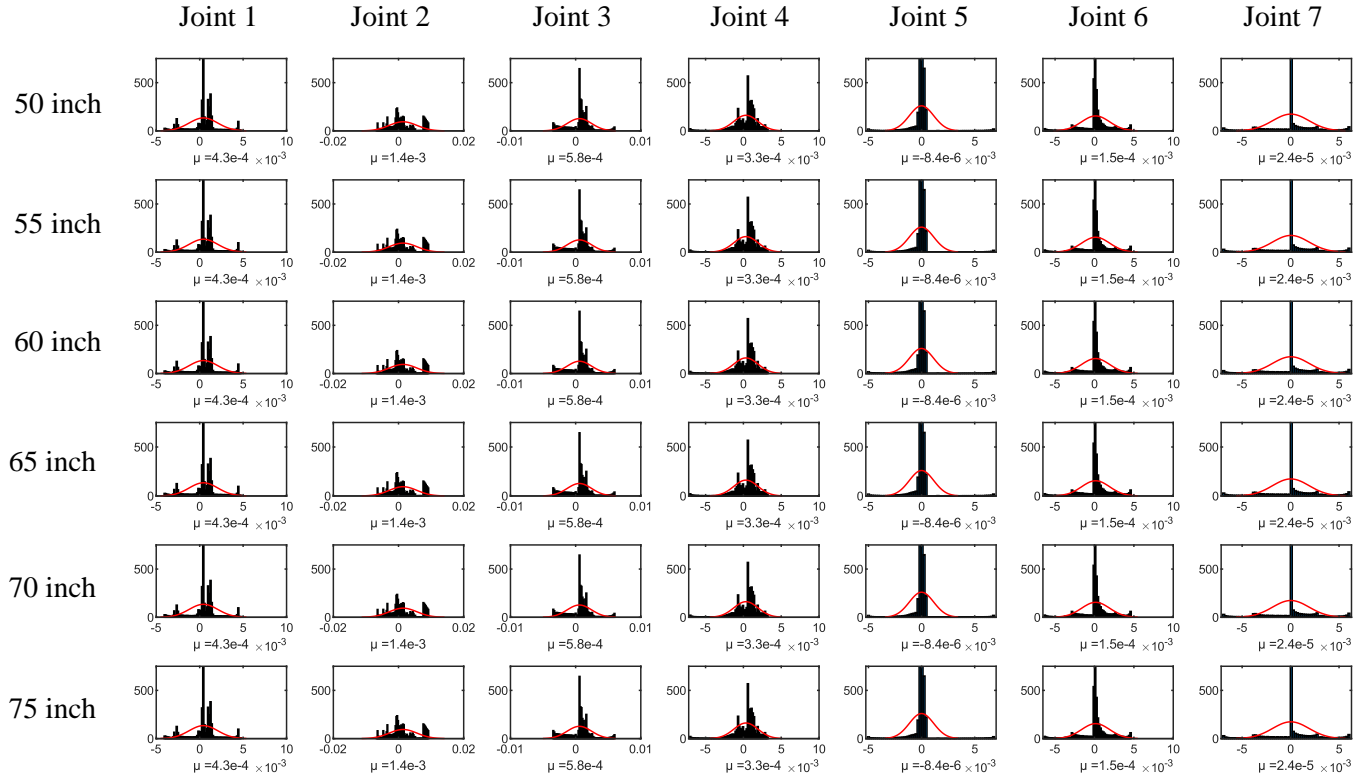
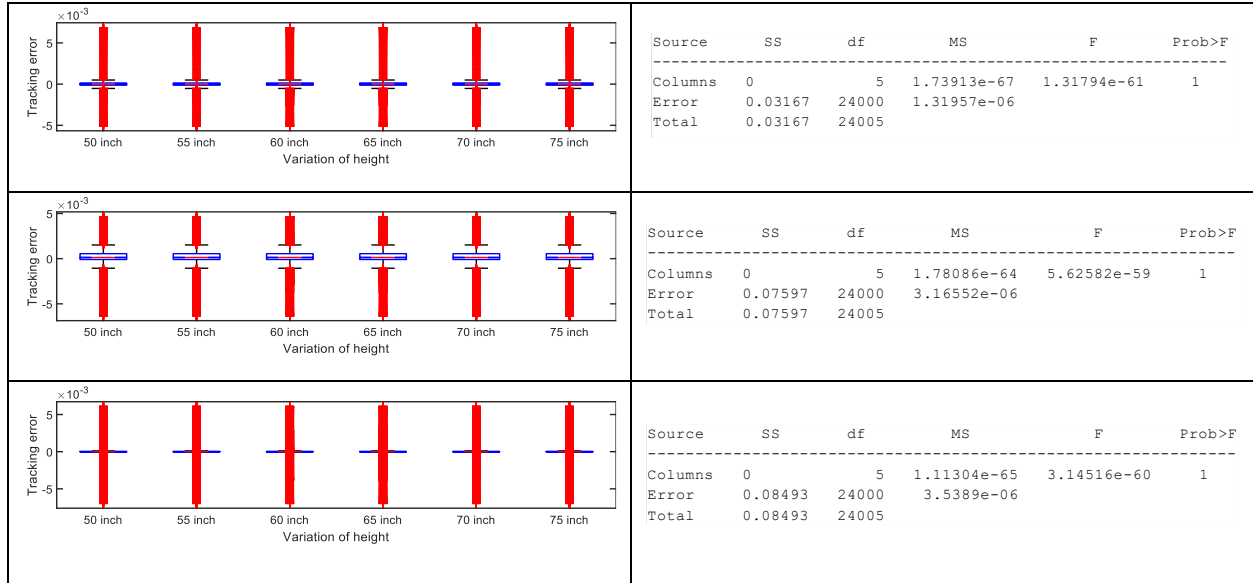


Figure 22 Tracking error distribution concerning the user's height variation

Table 4 Tracking error variation concerning the user's height

	<table><tr><th>Source</th><th>SS</th><th>df</th><th>MS</th><th>F</th><th>Prob&gt;F</th></tr><tr><td>Columns</td><td>0</td><td>5</td><td>0</td><td>0</td><td>1</td></tr><tr><td>Error</td><td>0.06521</td><td>24000</td><td>0.000003</td><td></td><td></td></tr><tr><td>Total</td><td>0.06521</td><td>24005</td><td></td><td></td><td></td></tr></table>	Source	SS	df	MS	F	Prob>F	Columns	0	5	0	0	1	Error	0.06521	24000	0.000003			Total	0.06521	24005			
Source	SS	df	MS	F	Prob>F																				
Columns	0	5	0	0	1																				
Error	0.06521	24000	0.000003																						
Total	0.06521	24005																							
	<table><tr><th>Source</th><th>SS</th><th>df</th><th>MS</th><th>F</th><th>Prob&gt;F</th></tr><tr><td>Columns</td><td>0</td><td>5</td><td>0</td><td>0</td><td>1</td></tr><tr><td>Error</td><td>0.43154</td><td>24000</td><td>0.000018</td><td></td><td></td></tr><tr><td>Total</td><td>0.43154</td><td>24005</td><td></td><td></td><td></td></tr></table>	Source	SS	df	MS	F	Prob>F	Columns	0	5	0	0	1	Error	0.43154	24000	0.000018			Total	0.43154	24005			
Source	SS	df	MS	F	Prob>F																				
Columns	0	5	0	0	1																				
Error	0.43154	24000	0.000018																						
Total	0.43154	24005																							
	<table><tr><th>Source</th><th>SS</th><th>df</th><th>MS</th><th>F</th><th>Prob&gt;F</th></tr><tr><td>Columns</td><td>0</td><td>5</td><td>0</td><td>0</td><td>1</td></tr><tr><td>Error</td><td>0.06134</td><td>24000</td><td>0.000003</td><td></td><td></td></tr><tr><td>Total</td><td>0.06134</td><td>24005</td><td></td><td></td><td></td></tr></table>	Source	SS	df	MS	F	Prob>F	Columns	0	5	0	0	1	Error	0.06134	24000	0.000003			Total	0.06134	24005			
Source	SS	df	MS	F	Prob>F																				
Columns	0	5	0	0	1																				
Error	0.06134	24000	0.000003																						
Total	0.06134	24005																							
	<table><tr><th>Source</th><th>SS</th><th>df</th><th>MS</th><th>F</th><th>Prob&gt;F</th></tr><tr><td>Columns</td><td>0</td><td>5</td><td>0</td><td>0</td><td>1</td></tr><tr><td>Error</td><td>0.06134</td><td>24000</td><td>0.000003</td><td></td><td></td></tr><tr><td>Total</td><td>0.06134</td><td>24005</td><td></td><td></td><td></td></tr></table>	Source	SS	df	MS	F	Prob>F	Columns	0	5	0	0	1	Error	0.06134	24000	0.000003			Total	0.06134	24005			
Source	SS	df	MS	F	Prob>F																				
Columns	0	5	0	0	1																				
Error	0.06134	24000	0.000003																						
Total	0.06134	24005																							



The next section will present the comparative studies between the developed controller and Sliding mode controller, Computed Torque Controller, Adaptive controller, Linear Quadratic Regulator, and Model Reference Computed Torque Controller.

## 8. Performance comparison of the developed deep learning technique-based controller with SMC, MRCTC, Adaptive controller, LQR

Figure 23 presents a generalized trajectory tracking performance of the Sliding Mode Controller, Computed Torque Controller, Adaptive controller, Linear Quadratic Regulator, and Model Reference Computed Torque Controller. It is difficult to show the details of 5 different controllers' performances in one paper. But if the readers are interested they can find the details of all 4 controllers in the following references [20], [18], [17], [19]. All four controllers are based on the same plant dynamics. By comparing

the controllers, it has been noticed that all the controller's trajectory tracking performance is very high and the amount of trajectory tracking torque required was very close.

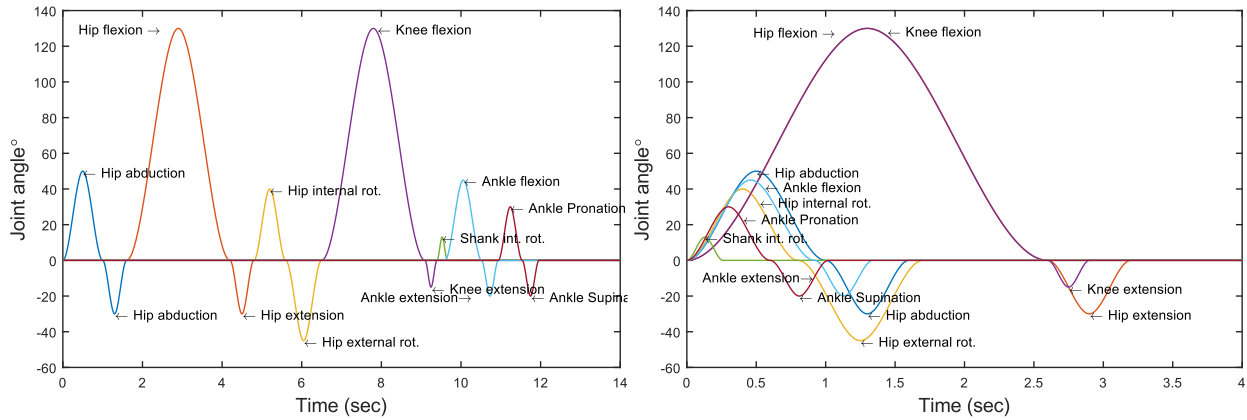


Figure 23 Trajectory tracking performance for the sequential joint movements (left) , simultaneous joint movements (right)

## 9. Conclusion

Deep neural networks are increasingly being used in the field of dynamic modeling and control. The main reason for the popularity of the deep neural network is that the trained network is computationally light in weight and can model dynamical behaviors accurately. In this article, a human lower extremity dynamic model was developed. To control the dynamical model, a computed torque controller was used. The developed dynamical system was simulated for a different combination of trajectories and user weight and height. Reference trajectories and plant input torques were used to generate the training data for the training of the proposed neural network. A four-layers deep neural network was developed for predicting the robot joint torques based on the reference trajectories and the user's weight and height. The developed deep neural network-based controller showed very high trajectory tracking accuracy. The stability analysis of the controller is presented. To verify the robustness of the developed controller to parameter variation ANOVA was performed. Finally, the performance of the developed controller was compared with Sliding Mode Controller, Computed Torque Controller, Adaptive controller, Linear Quadratic Regulator, and Model Reference Computed Torque Controller while keeping the robot dynamics the same.

## Reference

1. Javaid, M., et al., Substantial capabilities of robotics in enhancing industry 4.0 implementation. *Cognitive Robotics*, 2021. 1: p. 58-75.
2. Kyrarini, M., et al., A Survey of Robots in Healthcare. *Technologies*, 2021. 9(1): p. 8.
3. Gao, Y. and S. Chien, Review on space robotics: Toward top-level science through space exploration. *Science Robotics*, 2017. 2(7): p. ean5074.
4. Oliveira, L.F.P., A.P. Moreira, and M.F. Silva, Advances in Agriculture Robotics: A State-of-the-Art Review and Challenges Ahead. *Robotics*, 2021. 10(2): p. 52.
5. Bogue, R., Underwater robots: a review of technologies and applications. *Industrial Robot: An International Journal*, 2015. 42(3): p. 186-191.
6. Wang, Z., S. Hirai, and S. Kawamura, Challenges and Opportunities in Robotic Food Handling: A Review. *Frontiers in Robotics and AI*, 2022. 8.
7. Ji, W. and L. Wang, Industrial robotic machining: a review. *The International Journal of Advanced Manufacturing Technology*, 2019. 103(1): p. 1239-1255.
8. Hentout, A., et al., Human–robot interaction in industrial collaborative robotics: a literature review of the decade 2008–2017. *Advanced Robotics*, 2019. 33(15-16): p. 764-799.
9. Sapaty, P., Military Robotics: Latest Trends and Spatial Grasp Solutions. *International Journal of Advanced Research in Artificial Intelligence*, 2015. 4.
10. Gull, M.A., S. Bai, and T. Bak, A Review on Design of Upper Limb Exoskeletons. *Robotics*, 2020. 9(1): p. 16.
11. Yan, T., et al., Review of assistive strategies in powered lower-limb orthoses and exoskeletons. *Robotics and Autonomous Systems*, 2015. 64: p. 120-136.
12. Rodríguez-Fernández, A., J. Lobo-Prat, and J.M. Font-Llagunes, Systematic review on wearable lower-limb exoskeletons for gait training in neuromuscular impairments. *Journal of NeuroEngineering and Rehabilitation*, 2021. 18(1): p. 22.
13. Inkulu, A.K., et al., Challenges and opportunities in human robot collaboration context of Industry 4.0 - a state of the art review. *Industrial Robot: the international journal of robotics research and application*, 2022. 49(2): p. 226-239.
14. Nguyen-Tuong, D. and J. Peters, Model learning for robot control: A survey. *Cognitive processing*, 2011. 12: p. 319-40.
15. Craig, J.J., *Introduction to robotics : mechanics and control*. 2005: Pearson/Prentice Hall, Upper Saddle River, N.J.
16. Hasan, S.K. and A.K. Dhingra, Performance verification of different control schemes in human lower extremity rehabilitation robot. *Results in Control and Optimization*, 2021. 4: p. 100028.



17. Hasan, S.K. and A.K. Dhingra, An adaptive controller for human lower extremity exoskeleton robot. *Microsystem Technologies*, 2021. 27(7): p. 2829-2846.
18. Hasan, S.K. and A.K. Dhingra, Development of a model reference computed torque controller for a human lower extremity exoskeleton robot. *Proceedings of the Institution of Mechanical Engineers, Part I: Journal of Systems and Control Engineering*, 2021. 235(9): p. 1615-1637.
19. Hasan, S.K. and A. Dhingra, Developing a Linear Quadratic Regulator for Human Lower Extremity Exoskeleton Robot. *Journal of Mechatronics and Robotics*, 2022. 6(1).
20. Hasan, S.K. and A.K. Dhingra, Development of a sliding mode controller with chattering suppressor for human lower extremity exoskeleton robot. *Results in Control and Optimization*, 2022. 7: p. 100123.
21. Goodfellow, I.B. Y.C.A., *Deep learning*. 2016.
22. Dargan, S., et al., A Survey of Deep Learning and Its Applications: A New Paradigm to Machine Learning. *Archives of Computational Methods in Engineering*, 2020. 27(4): p. 1071-1092.
23. Chen, S. and J.T. Wen, Industrial Robot Trajectory Tracking Control Using Multi-Layer Neural Networks Trained by Iterative Learning Control. *Robotics*, 2021. 10(1): p. 50.
24. Zhihong, S. and K. Khorasani, A neural-network-based controller for a single-link flexible manipulator using the inverse dynamics approach. *IEEE Transactions on Industrial Electronics*, 2001. 48(6): p. 1074-1086.
25. Meng, Q., et al., Motion Planning and Adaptive Neural Tracking Control of an Uncertain Two-Link Rigid-Flexible Manipulator With Vibration Amplitude Constraint. *IEEE Transactions on Neural Networks and Learning Systems*, 2021: p. 1-15.
26. Talebi, H.A., K. Khorasani, and R.V. Patel, Neural network based control schemes for flexible-link manipulators: simulations and experiments. *Neural Netw*, 1998. 11(7-8): p. 1357-1377.
27. Yeşildirek, A., M.W. Vandegrift, and F.L. Lewis, A neural network controller for flexible-link robots. *Journal of Intelligent and Robotic Systems*, 1996. 17(4): p. 327-349.
28. Gao, H., et al., Neural Network Control of a Two-Link Flexible Robotic Manipulator Using Assumed Mode Method. *IEEE Transactions on Industrial Informatics*, 2019. 15(2): p. 755-765.
29. Yang, S., et al., An optimal fuzzy-theoretic setting of adaptive robust control design for a lower limb exoskeleton robot system. *Mechanical Systems and Signal Processing*, 2020. 141: p. 106706.
30. Ren, Y., et al., Adaptive Neural-Network Boundary Control for a Flexible Manipulator With Input Constraints and Model Uncertainties. *IEEE Transactions on Cybernetics*, 2021. 51(10): p. 4796-4807.
31. Lin, H., et al., Learning Deep Nets for Gravitational Dynamics With Unknown Disturbance Through Physical Knowledge Distillation: Initial Feasibility Study. *IEEE Robotics and Automation Letters*, 2021. 6(2): p. 2658-2665.

32. Mukhopadhyay, R., et al. Model Learning for Robotic Manipulators using Recurrent Neural Networks. in TENCON 2019 - 2019 IEEE Region 10 Conference (TENCON). 2019.
33. Liu, N., et al., Modeling and Simulation of Robot Inverse Dynamics Using LSTM-Based Deep Learning Algorithm for Smart Cities and Factories. IEEE Access, 2019. 7: p. 173989-173998.
34. Liang, B., et al. Robot Arm Dynamics Control Based on Deep Learning and Physical Simulation. in 2018 37th Chinese Control Conference (CCC). 2018.
35. Panwar, R. and N. Sukavanam, Trajectory tracking using artificial neural network for stable human-like gait with upper body motion. Neural Computing and Applications, 2020. 32(7): p. 2601-2619.
36. Narendra, K.S. and K. Parthasarathy, Identification and control of dynamical systems using neural networks. IEEE Transactions on Neural Networks, 1990. 1(1): p. 4-27.
37. Polydoros, A.S., L. Nalpantidis, and V. Krüger. Real-time deep learning of robotic manipulator inverse dynamics. in 2015 IEEE/RSJ International Conference on Intelligent Robots and Systems (IROS). 2015.
38. Liu, C., Z. Zhao, and G. Wen, Adaptive neural network control with optimal number of hidden nodes for trajectory tracking of robot manipulators. Neurocomputing, 2019. 350: p. 136-145.
39. He, W., Y. Dong, and C. Sun, Adaptive Neural Impedance Control of a Robotic Manipulator With Input Saturation. IEEE Transactions on Systems, Man, and Cybernetics: Systems, 2016. 46(3): p. 334-344.
40. Sanner, R.M. and J.J.E. Slotine, Gaussian networks for direct adaptive control. IEEE Transactions on Neural Networks, 1992. 3(6): p. 837-863.
41. Wu, Y., et al., Adaptive neural network control of uncertain robotic manipulators with external disturbance and time-varying output constraints. Neurocomputing, 2019. 323: p. 108-116.
42. Zhu, Q., Y. Liu, and G. Wen, Adaptive neural network control for time-varying state constrained nonlinear stochastic systems with input saturation. Information Sciences, 2020. 527: p. 191-209.
43. Mathworks.com. Friction in contact between rotating bodies. 2020 07/01/2020]; Available from: <https://www.mathworks.com/help/physmod/simscape/ref/rotationalfriction.html>.
44. Bengio, Y., Learning Deep Architectures for AI. Found. Trends Mach. Learn., 2009. 2(1): p. 1–127.
45. Hasan, S.K. and A.K. Dhingra, 8 Degrees of freedom human lower extremity kinematic and dynamic model development and control for exoskeleton robot based physical therapy. International Journal of Dynamics and Control, 2020.
46. Fisher, R.A., Statistical Methods for Research Workers, in Breakthroughs in Statistics: Methodology and Distribution, S. Kotz and N.L. Johnson, Editors. 1992, Springer New York: New York, NY. p. 66-70.

## List of Figures

Figure 1 Mechatronics architecture of a robot .....	3
Figure 2 Link Frame assignment based on modified D-H parameter .....	7
Figure 3 Internal architecture of the robot model .....	11
Figure 4 Internal architecture of the physical Robot model.....	11
Figure 5 Friction model simulation.....	13
Figure 6 Computed torque control scheme .....	14
Figure 7 Architecture of the developed neural network.....	15
Figure 8 Developed deep neural network for joint torque estimation.....	16
Figure 9 Hierarchical data generation schematic diagram .....	17
Figure 10 Input and Output data tracing locations in the simulation .....	18
Figure 11 Simultaneous and sequential joint movements (constructed based on the human lower extremity's full ranges of motion [45]) .....	19
Figure 12 Training Neural network .....	20
Figure 13 Control architecture of the Deep neural network-based robot controller .....	20
Figure 14 Architecture of the hybrid controller .....	21
Figure 15 Trajectory tracking performance (Simultaneous joint movement).....	22
Figure 16 Trajectory tracking Error (Simultaneous joint movement).....	22
Figure 17 From the top: total Joint torque requirement for sequential joint movements, Predicted torque, PD controller's contribution .....	23
Figure 18 Trajectory tracking performance (Sequential joint movements) .....	24
Figure 19 Trajectory tracking performance (Sequential joint movements) .....	24
Figure 20 From the left: total Joint torque requirement for sequential joint movements, DNN Predicted torque, PD controller's contribution .....	25
Figure 21 Tracking error distribution concerning weight variation.....	27
Figure 22 Tracking error distribution concerning the user's height variation .....	29

Figure 23 Trajectory tracking performance for the sequential joint movements (left) , simultaneous joint movements (right).....	31
---	----

## List of Tables

Table 1: Human lower extremity DH parameters .....	7
Table 2 Different values of joints velocities, subject's weight and height used for input data generation .	19
Table 3 Tracking error variation concerning the user's weight.....	27
Table 4 Tracking error variation concerning the user's height.....	29